Electronic Supplementary Material (ESI) for Nanoscale.
This journal is © The Royal Society of Chemistry 2024

Supporting Information:

Seeding the vertical growth of laterally coherent coordination polymers on the *rutile*-TiO_2(110) surface

Luca Schio,[§a] Gregor Bavdek,[§a,b] Cesare Grazioli,[a] Claudia Obersnù,[a,c] Albano Cossaro,[a,c] Andrea Goldoni,[d] Alberto Calloni,[e] Alberto Bossi,[f] Gianlorenzo Bussetti,[f] Alessio Orbelli Biroli,[g] Andrea Vittadini,[h] Luca Floreano*[a]*

[§] These two Authors contributed equally to the manuscript.
[a] CNR - Istituto Officina dei Materiali (IOM), Laboratorio TASC, Trieste, Italy.
[b] Didactic Faculty, University of Ljubljana, Ljubljana, Slovenia.
[c] Department of Chemical and Pharmaceutical Sciences, University of Trieste, Trieste, Italy
[d] Elettra-Sincrotrone Trieste S.C.p.A., Trieste, Italy.
[e] Physics Department, Politecnico di Milano, Milano, Italy.
[f] CNR-SCITEC and SmartMatLab, Milano, Italy.
[g] Chemistry Department, University of Pavia, Pavia, Italy.
[h] CNR-ICMATE and Department of Chemical Sciences, University of Padova, Padova, Italy.

Corresponding Authors

* E-mails: floreano@iom.cnr.it, andrea.vittadini@unipd.it

SUMMARY

Section S1: DFT calculations.

Section S2: Pyridine/M-TPP adducts in Gas phase.

Section S3: M-TPP^{ads} in the (2x4)-*oblique* phase.

Section S4: Experimental methods: XPS and NEXAFS.

Section S5: Sample preparation.

Section S6: Characterization of DPNDI on TiO_2(110).

Section S7: Characterization of bipyridine on TiO_2(110).

S1. DFT calculations.

DFT calculations were performed using the Quantum ESPRESSO package.[1] The PBE functional[2] was adopted in conjuction with D2 Grimme dispersion.[3],[4] Ion cores were described by Vanderbilt ultrasoft pseudopotentials,[5] which included C, N, and O 1s electrons and Ti 1*s*-2*p* electrons. Valence orbitals were expanded on a plane-wave basis set with kinetic energy cutoff of 25 Ry, while the cutoff on the augmentation density was 200 Ry. Gas phase molecules were placed in large supercells, whereas adsorbed molecules where placed in slabs of ten unit cells and six TiO_2 layers.

S2. Pyridine/M-TPP adducts in the Gas phase: binding energy and equilibrium distance.

In our DFT calculations we model the DPNDI ligand with a simple pyridine (Py) molecule, while the TiO_2(110) surface is represented by a periodically repeated slab. There is possibly an interplay between the interactions involving the M-TPP species with the TiO_2 surface and with pyridine. In fact, on one hand, the metal ion M can play a direct role in O_{br}-M and in M-N^{Py} bonds. On the other hand, the saddle deformation of the M-TPP species induced by the adsorption to the surface may in turn influence the interaction between the whole M-TPP moiety and the pyridine ring. In order to disentangle these effects, we carried out three series of calculations where only two or all the components of the triad were included.

We first examine the formation of Py/M-TPP adducts in the gas phase. The pyridine molecular plane is perpendicular to that of the porphyrin N_4 chromophore, with the N(Py) atom on top of the metal ion, as previously found for similar adducts (*e.g.* Ref. [6]). We computed the pyridine to M-TPP binding energy E_b(Py) from total energies E as follows:

$$E_b(Py) = E[Py/M\text{-}TPP] - E[M\text{-}TPP] - E[Py] \quad , \qquad (1)$$

where all the species are placed in large supercells to simulate the gas phase.

Table S1. Pyridine binding energies, E_b(Py), for Py/M-TPP adducts formed in the gas phase; the corresponding equilibrium distances between the metal and pyridine N atom, M-N^{Py}, are also shown together with the average distance between the metal and the chelated N atoms, M-N_4, as measured in bulk MTPP.

	E_b(Py) gas phase	Calc. d(M-N^{Py}) gas phase	Exp. d(M-N_4) M-TPP bulk
Co-TPP	-0.99 eV	2.11 Å	1.95 Å *
Zn-TPP	-0.78 eV	2.19 Å	2.04 Å **
Cu-TPP	-0.45 eV	2.33 Å	1.98 Å **
Ni-TPP	-0.26 eV	2.48 Å	1.93 Å ***

* Refs. [7],[8]
** Ref. [9]
*** Ref. [10]

The obtained results (shown in Table S1) compare well with B3LYP calculations previously carried out on adducts formed between pyridine and Cu and Zn metalloporphyrin (M-TPP) complexes,[11] predicting E_b(Py)= 0.57 eV and d[M-N^{Py}] =2.35 Å for Cu-Porphyrin, and E_b(Py)= 0.93 eV, d[M-N^{Py}] =2.18 Å for Zn-Porphyrin. As a whole, our data show an almost linear correlation between the M-N^{Py} distance and the strength of the N^{Py}/M-TPP interaction, where the latter is markedly higher in the Zn and the Co case.

S3. M-TPP^{ads} in the (2x4)-*oblique* phase: adsorption site and energy.

In Ref. [12], DFT calculations were used to study the structure and the stability of M-TPP (M = Co, Ni, Cu, Zn) complexes adsorbed at the Ti-top, Ti-bridge, O-top, and O-bridge sites of the TiO_2(110) surface. Large supercells were adopted, to avoid interactions between the M-TPP species and their periodic images. This allows exploring the stability of the adsorbate as a function of the azimuthal orientation, which is essential as species adsorbed at different sites have in principles different azimuthal preferences. In fact, it was found that Co-TPP and Zn-TPP prefer the O_{br}-top site forming a M-O_{br} bond, whereas Ni-TPP and Cu-TPP, whose cations cannot interact with the surface anions, have a slight preference for the O_{br}-bridge configuration, similar to the 2H-TPP free-base.

The O_{br}-top/O_{br}-bridge configurations are more stable by 0.6-0.8 eV with respect to local minima on sites at the Ti_{5f} rows, where the species are rotated by 45°.

Adsorption of 2H-TPP species at TiO_2(110) has been shown to form densely packed phases, where the structure, characterized by saddle-deformed species adsorbed at O_{br}-row sites, is not significantly modified with respect that observed for the isolated species.[13],[14] Because these phases are described by smaller supercells, they can be used to study chemical processes undergone by 2H-TPP species adsorbed at TiO_2(110) at a reduced computational cost. In fact, this was done in a previous investigation on the self-metalation reaction of 2H-TPP where a $\begin{bmatrix} 2 & -2 \\ 1 & 4 \end{bmatrix}$ supercell was used.[15]

Because the MTPP species adsorbed at TiO_2(110) give rise to the same phases observed for the 2H-TPP ones, we decided to adopt the same supercell used in Ref. [15] to study the interaction between the adsorbed M-TPP species and pyridine. This allows to compensate the larger computational cost due to the increased thickness of the slab required to accommodate the pyridine ligand. All M-TPP species have been placed both at the O_{br}-bridge and at O_{br}-top sites while the adsorption energies were computed as:

$$E_{ads}(\text{M-TPP}) = E(\text{M-TPP}^{ads}) - E(\text{Surf}) - E(\text{M-TPP}), \qquad (2)$$

where Surf stands for the slab describing the clean TiO_2(110) surface, M-TPP^{ads} indicates the slab modeling the M-TPP species adsorbed at the surface, and M-TPP is the molecule in the gas phase.

Table S2. Adsorption energies and M-O_{br} distances for complexes adsorbed on different sites at the O_{br}-row of the TiO_2(110) surface arranged in a densely packed (2x4)-*oblique* phase.

	E_{ads}(M-TPP) [eV]		d(M-O_{br}) [Å]	
	M-TPP@O_{br}-top	M-TPP@O_{br}-bridge	M-TPP@O_{br}-top	M-TPP@O_{br}-bridge
Co-TPP	-3.48	-3.16	2.29	3.01
Ni-TPP	-3.24	-3.25	2.71	3.10
Cu-TPP	-3.22	-3.16	2.70	3.10
Zn-TPP	-3.16	-2.99	2.26	3.02

When compared with data relative to "isolated" adsorbed molecules reported in Ref. [12], the present results (see Table S2) show a slight stabilization for all the configurations, which is generally stronger for the O_{br}-top ones. Hence, the O_{br}-top site remains preferred for Co-TPP and Zn-TPP, whereas no clear site preference can be predicted for Ni-TPP and Cu-TPP. We point out that the stabilization of O-$_{br}$top sites is to be ascribed to additional or stronger surface-ligand and/or ligand-ligand van der Waals interactions allowed by the high density of the phase. In fact, similar to the isolated molecule case, no significant Cu-O_{br} and Ni-O_{br} interactions are present, as it can be deduced by large the M-O_{br} distances for the O_{br}-top configurations.

S4. Experimental methods (XPS and NEXAFS) and instrumental setup.

All the experiments (but the study of bipyridine/TiO_2 of section S7) were performed at the main endstation of the ALOISA beamline. X-ray photoemission spectra have been measured with the sample at a grazing angle of 4.0˚ (*p*-polarization) and near normal emission. We used a hemispherical analyzer (mean radius of 66 mm, acceptance angle of ~2˚ FWHM) equipped with multichannel plates coupled to a 2D delay line detector (2 MHz dynamical range). We measured XPS at photon energies of 650 eV (O 1s, Ti 2p, N 1s, C 1s, Ti 3p) and 515 eV (N 1s, C 1s, Ti 3p) with an overall energy resolution of ~200 and ~160 meV, respectively. The photoemission spectra have been calibrated to the Binding Energy of Ti(IV) $2p_{3/2}$ and 3p at 459.1 and 37.6 eV, respectively. All XPS measurements have been performed with the photon beam along the [100] direction, i.e. parallel to the O_{br} rows.

NEXAFS spectra have been measured keeping the sample at a constant grazing angle of 6.0˚ and rotating the surface around the photon beam axis for changing the surface orientation with respect to the photon beam linear polarization. Unless otherwise specified (see next section S6), all NEXAFS spectra shown in the manuscript and hereafter have been measured with the surface [100] direction (O_{br} rows) oriented along the photon beam. The N *K*-edge spectra have been measured by scanning the photon energy together with the Undulator source and monitoring the drain current (i0) on the Au coating of the last (refocusing) mirror behind the exit slits. We measured NEXAFS in partial electron yield by means of a channeltron equipped with a frontal grid (repeller) biased at -370 V to reject low energy secondary electrons. We performed *a posteriori* an absolute photon energy calibration (better than 20 meV) by alignment of the N absorption features of the i0 with simultaneous gas phase NEXAFS measurements of N_2 in a windowless in-line gas ionization cell,[16] as shown in next Fig. S1.

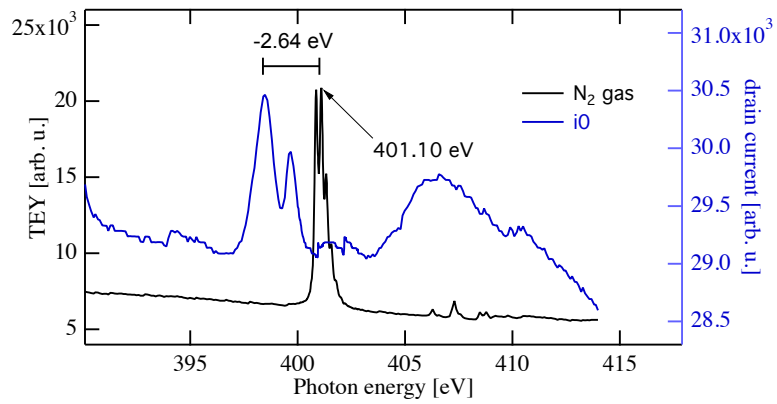

Fig. S1. Simultaneous acquisition of the N 1s → π* transition of gaseous N_2 (black curve) and drain current i0 (blue curve) with the ALOISA in-line windowless gas ionization cell. Partial electron yield is measured by means of a channeltron in a differentially pumped chamber in between the exit slits and the last refocusing mirror. The photon energy calibration of the i0 absorption features due to N contamination of the optical surface is made with reference to the absolute energy of the second vibrational line at 401.10 eV of the N 1s → π* transition.

Because of instabilities of the electron beam orbit in the storage ring during the Run of experiments, we normalized the spectra to a linear extrapolation of the pre-edge, rather than to reference spectra measured on the clean substrate. This protocol yielded lower noise without affecting the fine structure of resonances, thanks to the very high flux transmission of the ALOISA beamline at the N *K*-edge (>99%), as shown in the following Fig. S2.

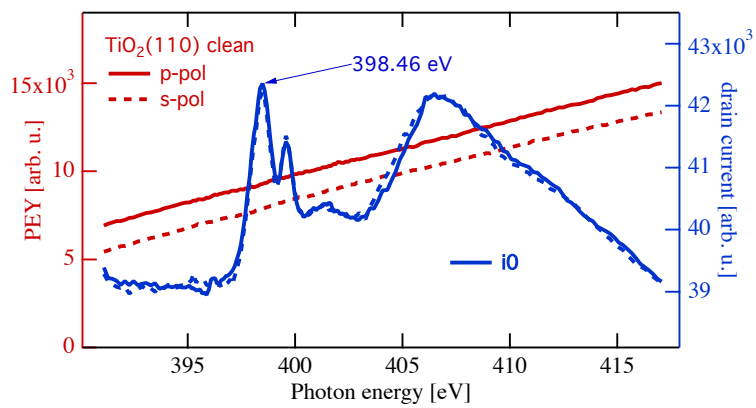

Fig. S2. Left axis: reference NEXAFS measurements on the clean TiO_2(110) surface in *p*- and *s*-polarization (full and dashed red lines, respectively); the scale range, starting at zero, lets the reader appreciate the flat beamline transmission at the N *K*-edge. Right axis: the corresponding simultaneous measurements of the drain current i0 (blue lines) on the last refocusing mirror are shown in an enhanced scale to highlight the absorption features due to adsorbate contaminants, which are used for absolute calibration of the photon energy.

S5. Sample preparation.

Experiments were performed on a circular *rutile*-TiO_2(110) sample (purchased from Pi-Kem) with diameter of 8 mm and thickness of 0.5 mm. The sample was glued by silver paste on a thin (1 mm) molybdenum spacer and put on the sample holder with Mo clips. The sample holder is equipped with two thermocouples in mechanical contact with the Mo spacer and carries one filament underneath the Mo spacer for radiative (up to 500˚C) and/or electron bombardment heating (up to 800˚C). The sample had already been processed in UHV and was dark blue when inserted in the preparation chamber. After each experiment, the sample was cleaned by two

cycles of Ar^+ ion sputtering at 1.5 kV at room temperature, RT, followed by short time (1 min) annealing to 680˚C. The sample holder is mounted on a six-degrees of freedom manipulator that is installed coaxially to the photon beam. The sample is moved forth and back from the preparation chamber (base pressure of $2x10^{-10}$ mbar) to the experimental one (base pressure in 10^{-11} mbar range). The preparation chamber is equipped with standard UHV equipment for sample cleaning (ion gun, gas lines, RGA), a RHEED system is used for sample alignment and check of crystal ordering. A molecular beam epitaxy (MBE) cryopanel (water cooling), equipped with four slots for evaporation cells, shutters and microbalances, is also installed in the preparation chamber. All molecules were loaded into a commercial 4-cells Kentax evaporator (quartz crucibles) installed into a single MBE slot.

We have recently reported on the sticking on TiO_2(110) of contaminants present in commercially available porphyrin powders. We refer to the SI file of our Ref. [12] for XPS spectra and details, while here we just recall that small fragments of pyrrolic nature are mostly desorbed by postdeposition mild annealing to 70-80˚C. In the present Run of experiments at Synchrotron, we could sufficiently outgass the Zn-TPP powder, while Cu-TPP and Co-TPP still displayed the presence of some pyrrolic contaminants even after mild annealing to 70-80˚C. In fact, MTPPs may also display the presence of free-basis porphyrins (whose sublimation temperature is very close to that of M-TPPs), which directly stick to the surface, where they assume their acidic form 4H-TPP due to hydrogen capture, *i.e.* they would not display the iminic contribution.[13]

The deposition rate was controlled by means of a quartz microbalance brought in front of the Knudsen cells before and after deposition. The coverage was calibrated during the many experiments of porphyrin deposition performed at the ALOISA beamline. We adopted the same nominal molecular density of 1,32 g/mm^3 for all molecules (porphyrins and DPNDI), which yields the completion of 1 ML of M-TPPs at a nominal thickness of 2.8-3.0 Å (the microbalance is not cooled, hence a rate indetermination up to 5 % may be expected). We deposited Zn- Co- and Cu-TPP with the same nominal thickness of 2.8 Å (slightly less than 1 ML), in order to avoid second layer molecules that would automatically coordinate DPNDI at their out of plane axial site.

Concerning DPNDI, the nominal thickness corresponding to a 1:1 stoichiometric ratio with a 2.8 Å thickness of deposited M-TPP was found to correspond to ~1.9 Å. This value is in full agreement with the former value adopted for the DPNDI / Zn-TPP coordination on Fe(001)-*p*(1x1)O, where a saturated porphyrin monolayer was obtained by thermal desorption of a bi-layer.[17] In the case of Co-TPP, we deposited a lower amount of DPNDI (1.5Å), which takes into account the larger fraction of 2H-TPP contaminants (~20%) for achieving an effective 1:1 stoichiometric ratio with the fraction of metalated porphyrin.

We remark that the determination of the exact amount of DPNDI that can be accommodated in the first layer (*i.e.* its nominal thickness) on bare TiO_2(110) is not straightforward. The molecules initially grow closely parallel to the surface (2 Å), but, with increasing deposition (4 Å), one observes an increase of the molecular tilt (see NEXAFS study in next section S6). We attribute the tilting up of molecules to molecular side-by-side packing within the molecular layer, rather than to 2nd layer formation, because all molecules still display the spectroscopic fingerprint of substrate charge transfer at 4 Å. The DPNDI electronic decoupling from the substrate (and increase of tilt angle) proceeds gradually with further deposition. On the other hand, DPNDI reacts with the substrate upon mild annealing beyond 100-150˚C; the corresponding change of XPS and NEXAFS prevents a precise determination of the nominal thickness for a saturated monolayer (likely in the range of ~6 Å), as obtained by 2nd layer thermal desorption. Overall, DPNDI may reach a molecular density of the first layer much larger than that of M-TPPs. For this reason, non coordinated DPNDI may easily accommodate in between M-TPPs.

As highlighted in the main text, a significant charge transfer takes place at low coverage, which shifts the two distinct N 1s peaks of DPNDI to merge into a single broad peak. The C 1s XPS, shown in next Fig. S3, follows a trend opposite to that of N 1s in Fig. 2 of the main text. In the multilayer regime, the C 1s XPS closely matches that of PTCDI,[18] with a major component, contributed by both naphthalene and pyridine aromatic carbons, at a binding energy (BE) of 285.8 eV. At low coverage, the major component is split in two features at 284.5 and 286.0 eV, respectively. The imide component (O=C–N) at 288.9 eV is marginally affected by the charge transfer, displaying a small BE shift of ~0.3 eV to lower BE.

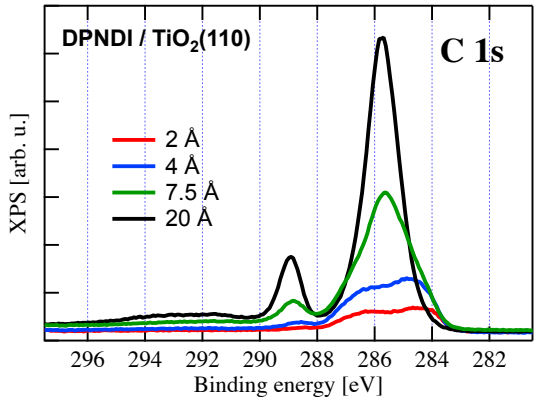

Fig. S3. C 1s photoemission spectra measured at a photon energy of 515 eV as a function of the DPNDI thickness on TiO_2(110) at room temperature; the overall energy resolution is ~160 meV.

S6. Characterization of DPNDI on TiO_2(110).

Thanks to the two-fold symmetry of the TiO_2(110) surface, we may use NEXAFS in *s*-polarization to get information about the azimuthal orientation of the DPNDI molecular plane with respect to the substrate O_{br} rows that extend along the [001] orientation (see Fig. 1). We have measured a complete set of NEXAFS on DPNDI directly deposited on TiO_2(110) at room temperature for a few representative film thicknesses (2, 4 and 20 Å), as shown in Fig. S4. The spectra in *s*-polarization have been measured with the photon beam oriented either along or transverse to the O_{br} rows. In the submonolayer range, we detected a clear azimuthal dichroism: the residual intensity of the π*-symmetry resonances, observed when the electric field is transverse to the O_{br} rows, completely vanishes when the electric field is parallel to them. This indicates that the DPNDI molecular axis is oriented parallel to the O_{br} rows, and the molecular plane is slightly tilted off the surface by rotation around the molecular axis. Overall molecules at low coverage are closely parallel to the surface, and they tilt off the surface with increasing coverage. We may infer that DPNDI molecules, initially growing with a very small tilt angle (<15˚), rise from the surface due to side-by-side coupling as the molecular density increases. In the multilayer range (20 Å) the linear dichroism strongly decreases and the azimuthal one vanishes, pointing to a closely random molecular orientation.

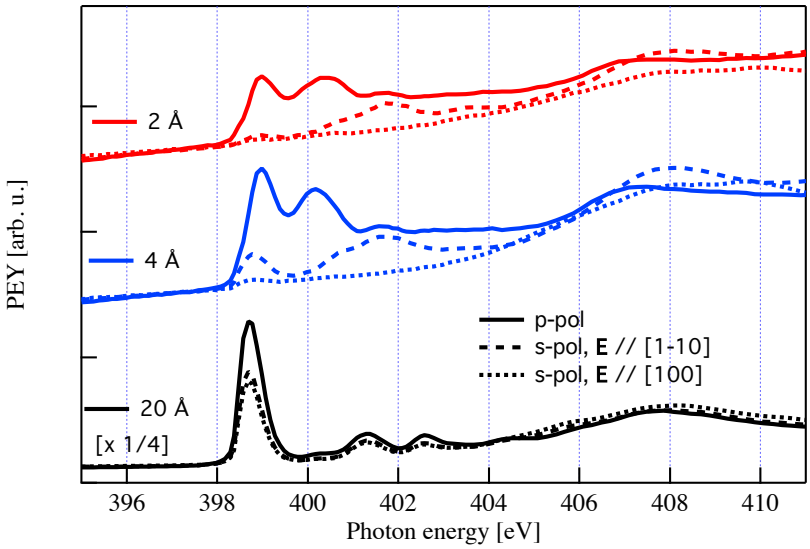

Fig. S4. Partial electron yield NEXAFS at the N *K*-edge (energy resolution of ~100 eV) from DPNDI deposited on TiO_2(110) at room temperature; the spectra have been measured at constant grazing angle (6.0˚) in *p*-polarization (full lines) and in *s*-polarization, with the electric field oriented either transverse (dashed lines) or parallel (dotted lines) to the O_{br} rows ([100] direction); the spectra at 2 and 4 Å are to scale, the spectra at 20 Å have been rescaled by a factor 1/4. All spectra are calibrated in energy (see section S4), but not otherwise normalized to the substrate and/or photon flux.

S7. Characterization of bipyridine on TiO_2(110).

We characterized bipyridine deposition on TiO_2(110) at the HASPES branchline of ALOISA,[19] where a 150mm analyzer is installed in a conventional geometrical setup: the analyzer is installed at 55˚ from the incoming photon beam and coupled to a six-degrees of freedom manipulator mounted vertically; the sample holder is exchangeable with the ALOISA one for a perfect reproducibility of temperature control, overall sample cleaning and preparation procedures.

The 4,4′-bipyridine molecules were evaporated from a Pyrex glass tube at room temperature. The sample was also kept at room temperature. The N 1s and C 1s photoemission spectra at different coverage are shown in Fig. S5. The coverage was estimated a posteriori by mild annealing a thicker film (1.5 ML) at 80˚C (orange line in Fig. S5), thus desorbing 2nd layer molecules with little changes in the contact layer. Higher annealing temperatures induce major changes in the XPS signal, which were not investigated further. The N and C 1s spectra show a close matching of the monolayer and multilayer binding energies; in particular the N 1s binding energy is found at 399.8-399.9 eV, in good agreement with former reports,[20] clearly indicating that no chemical bonds are formed with the TiO_2(110) surface at room temperature.

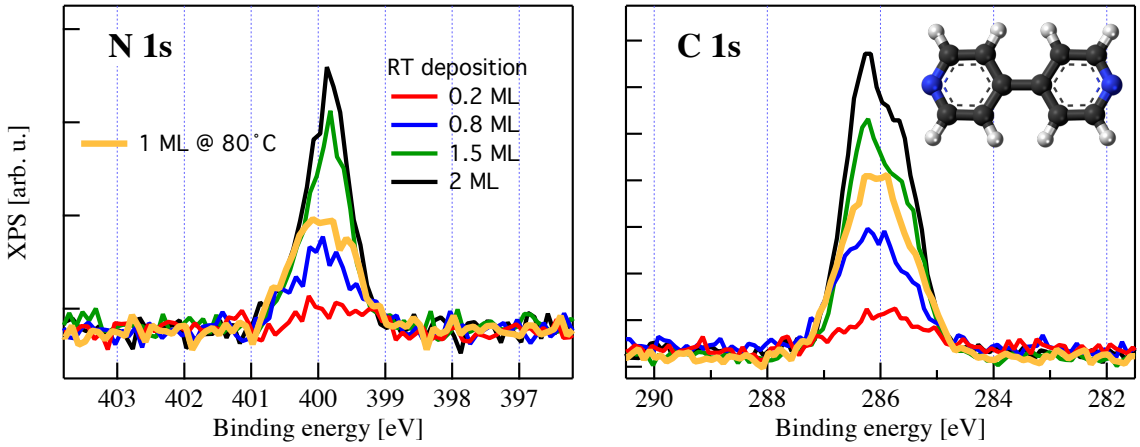

Fig. S5. XPS measured on bipyridine/TiO_2(110) with a photon energy of 650 eV and an overall energy resolution of ~200 meV. The spectra are calibrated in energy to the reference Ti(IV) $2p_{3/2}$ peak at 459.1 eV. The corresponding coverage is indicated in the left panel, with the same color code for both panels.

REFERENCES

[1] P. Giannozzi, O. Andreussi, T. Brumme, O. Bunau, M. Buongiorno Nardelli, M. Calandra, R. Car, C. Cavazzoni, D. Ceresoli, M. Cococcioni, N. Colonna, I. Carnimeo, A. Dal Corso, S. de Gironcoli, P. Delugas, R. A. DiStasio, A. Ferretti, A. Floris, G. Fratesi, G. Fugallo, R. Gebauer, U. Gerstmann, F. Giustino, T. Gorni, J. Jia, M. Kawamura, H.-Y. Ko, A. Kokalj, E. Küçükbenli, M. Lazzeri, M. Marsili, N. Marzari, F. Mauri, N. L. Nguyen, H.-V. Nguyen, A. Otero-de-la-Roza, L. Paulatto, S. Poncé, D. Rocca, R. Sabatini, B. Santra, M. Schlipf, A. P. Seitsonen, A. Smogunov, I. Timrov, T. Thonhauser, P. Umari, N. Vast, X. Wu, S. Baroni, *J. Phys. Condens. Matter* **2017**, *29*, 465901.

[2] J. P. Perdew, K. Burke, M. Ernzerhof, *Phys. Rev. Lett.* **1996**, *77*, 3865–3868.

[3] S. Grimme, *J. Comput. Chem.* **2006**, *27*, 1787–1799.

[4] V. Barone, M. Casarin, D. Forrer, M. Pavone, M. Sambi, A. Vittadini, *J. Comput. Chem.* **2009**, *30*, 934–939.

[5] D. Vanderbilt, *Phys. Rev. B* **1990**, *41*, 7892–7895.
[6] D. V Konarev, A. L. Litvinov, I. S. Neretin, N. V Drichko, Y. L. Slovokhotov, R. N. Lyubovskaya, J. A. K. Howard, D. S. Yufit, **2004**, *4*, 10–13.
[7] P. Madura, W. R. Scheldt, *Inorg. Chem.* **1976**, *15*, 3182–3184.
[8] E. D. Stevens, *J. Am. Chem. Soc.* **1981**, *103*, 5087–5095.
[9] E. B. Fleischer, C. K. Miller, L. E. Webb, *J. Am. Chem. Soc.* **1964**, *86*, 2342–2347.
[10] W. R. Scheidt, I. Turowska-tyrk, *Inorg. Chem.* **1994**, *33*, 1314–1318.
[11] J. Cremers, S. Richert, D. V. Kondratuk, T. D. W. Claridge, C. R. Timmel, H. L. Anderson, *Chem. Sci.* **2016**, *7*, 6961–6968.
[12] L. Schio, G. Bavdek, C. Grazioli, C. Gutiérrez Bolaños, A. Goldoni, A. Vittadini, M. Tormen, L. Floreano, *Appl. Surf. Sci.* **2023**, *616*, DOI 10.1016/j.apsusc.2023.156548.
[13] G. Lovat, D. Forrer, M. Abadia, M. Dominguez, M. Casarin, C. Rogero, A. Vittadini, L. Floreano, *Phys. Chem. Chem. Phys.* **2015**, *17*, 30119–30124.
[14] G. Lovat, D. Forrer, M. Abadia, M. Dominguez, M. Casarin, C. Rogero, A. Vittadini, L. Floreano, *J. Phys. Chem. C* **2017**, *121*, 13738–13746.
[15] M. K. Kremer, D. Forrer, C. Rogero, L. Floreano, A. Vittadini, *Appl. Surf. Sci.* **2021**, *564*, DOI 10.1016/j.apsusc.2021.150403.
[16] L. Floreano, G. Naletto, D. Cvetko, R. Gotter, M. Malvezzi, L. Marassi, A. Morgante, A. Santaniello, A. Verdini, F. Tommasini, G. Tondello, *Rev. Sci. Instrum.* **1999**, *70*, 3855–3864.
[17] A. Orbelli Biroli, A. Calloni, A. Bossi, M. S. Jagadeesh, G. Albani, L. Duò, F. Ciccacci, A. Goldoni, A. Verdini, L. Schio, L. Floreano, G. Bussetti, *Adv. Funct. Mater.* **2021**, *31*, 1–7.
[18] G. Fratesi, V. Lanzilotto, S. Stranges, M. Alagia, G. P. Brivio, L. Floreano, *Phys. Chem. Chem. Phys.* **2014**, *16*, 14834–14844.
[19] L. Floreano, A. Cossaro, R. Gotter, A. Verdini, G. Bavdek, F. Evangelista, A. Ruocco, A. Morgante, D. Cvetko, *J. Phys. Chem. C* **2008**, *112*, 10794–10802.
[20] A. Ravikumar, G. Kladnik, M. Müller, A. Cossaro, G. Bavdek, L. L. Patera, D. Sánchez-Portal, L. Venkataraman, A. Morgante, G. P. Brivio, D. Cvetko, G. Fratesi, *Nanoscale* **2018**, *10*, 8014–8022.